Results in Physics 8 (2018) 194–205

Contents lists available at ScienceDirect

Results in Physics

journal homepage: www.journals.elsevier.com/results-in-physics

A similarity solution of time dependent MHD liquid film flow over stretching sheet with variable physical properties

M. Idrees [a], Sajid Rehman [a,*], Rehan Ali Shah [b], M. Ullah [a], Tariq Abbas [c]

[a] Department of Mathematics, Islamia College Peshawar, Khyber Pakhtunkhwa, Pakistan
[b] Department of Basic Sciences and Islamiat, University of Engineering and Technology Peshawar, Khyber Pakhtunkhwa, Pakistan
[c] Department of Basic Sciences, Sarhad University Peshawar, Khyber Pakhtunkhwa, Pakistan

ARTICLE INFO

Article history:
Received 13 October 2017
Received in revised form 22 November 2017
Accepted 5 December 2017
Available online 9 December 2017

Keywords:
Variable viscosity and thermal conductivity
Thermocapillary number
Magnetic field
Thin film
Unsteady stretching surface

ABSTRACT

An analysis is performed for the fluid dynamics incorporating the variation of viscosity and thermal conductivity on an unsteady two-dimensional free surface flow of a viscous incompressible conducting fluid taking into account the effect of a magnetic field. Surface tension quadratically vary with temperature while fluid viscosity and thermal conductivity are assumed to vary as a linear function of temperature. The boundary layer partial differential equations in cartesian coordinates are transformed into a system of nonlinear ordinary differential equations (ODEs) by similarity transformation. The developed nonlinear equations are solved analytically by Homotopy Analysis Method (HAM) while numerically by using the shooting method. The Effects of natural parameters such as the variable viscosity parameter A, variable thermal conductivity parameter N, Hartmann number Ma, film Thickness, unsteadiness parameter S, Thermocapillary number M and Prandtl number Pr on the velocity and temperature profiles are investigated. The results for the surface skin friction coefficient $f''(0)$, Nusselt number (heat flux) $-\theta'(0)$ and free surface temperature $\theta(1)$ are presented graphically and in tabular form.

Introduction

In several engineering processes boundary layer flow and heat transfer phenomena of an unsteady free surface flow have promising applications such as continuous casting, wire coating, metal and polymer extrusion, foodstuff processing, drawing of plastic sheets, daily life uses equipments, etc. Crane [1] in 1970 is the first who studied the hydrodynamics of a steady stretching of a flat elastic sheet in a two-dimensional boundary layer flow by reducing the steady Navier-Stokes equations to a nonlinear ordinary differential equations by means of similarity transformation. Wang [2] in 1990 first studied the hydrodynamics of an unsteady stretching surface in a thin liquid film of a flow by converting the unsteady Navier-Stokes equations to a nonlinear ordinary differential equations by means of similarity transformation. But Lai and Kulacki [3] in 1991, assumed that viscosity and thermal conductivity are vary as an inverse functions of temperature and then solved numerically by using Runge-Kutta shooting method. Anderson et al. [4] in 2000, extend the work of Wang [2] by studying heat transfer and analysis has been performed by shooting method. Wang [5] in 2006, give analytical solution by using HAM [17] to the work of Anderson et al. [4] and found good agreement with multiple shooting method. Furthermore Seddeek and Faiza [6] in 2006, considered variable viscosity, variable thermal conductivity and variable suction with in Magneto Hydrodynamic (MHD) unsteady convective heat transfer along with semi-infinite vertical porous moving plate. Temperature variation phenomena in more general form introduced by Liu et al. [7] in 2008, in the work of Anderson et al. [4]. Mean while, Abel et al. [8] in 2008, introduce the magnetic field effect to the flow of an unsteady stretching surface in a thin liquid film and subsequent heat transfer from the stretching surface is investigated with the aid of similarity transformation, which is the extension of the work of Wang [2]. Moreover, unsteady stretching phenomena has been discussed with the effects of the thermocapillary number in the references [9–11]. More realistic approach was used by Yasir et al. [12] in 2011, by studying flow over stretching sheet by taking variable physical properties. For solution purpose they used HPM. Hazarika and Jadav Konch [13] in 2014, investigate the effects of varying thermal conductivity and viscosity, variable heat flux and constant suction on the MHD boundary layer flow forced convective past a stretching/shrinking sheet. Furthermore, the influence of MHD on fluid flow in various geometries was studied in [20–22]. These are vary

* Corresponding author.
E-mail address: sajid.rehman@icp.edu.pk (S. Rehman).

https://doi.org/10.1016/j.rinp.2017.12.009
2211-3797/

Nomenclature

N	thermal conductivity parameter
h_1	fluid constant
b	positive constant
t	time
u, v	x and y components of velocity
x, y	spatial Cartesian coordinates
Pr	Prandtl number
B	magnetic field
S	unsteadiness parameter
Ma	Hartmann number
$h(t)$	liquid film thickness
M	Thermocapillary number
T	temperature
T_0	temperature at the stretching sheet
T_s	temperature at the surface of fluid
T_{ref}	reference temperature
L	characteristic length scale
U	surface velocity
g	gravitational acceleration
A	viscosity parameter

Subscripts

ref	reference value
s	at the surface of fluid
0	at the stretching sheet
Re	Reynolds number

P_s	pressure at the surface of fluid
U_s	stretching surface velocity

Greek symbols

ß	thermal expansion coefficient
α	positive constant
β	dimensionless film thickness
ρ	density
δ	positive constant
κ	thermal conductivity
σ	surface tension
$\hat{\sigma}$	electrical conductivity
Υ	dimensionless film thickness
μ	viscosity
ν	kinematic viscosity
η	similarity variable
δ	positive fluid property
σ_0	surface tension at sheet
$\hat{\delta}$	characteristic length scale
θ	dimensionless temperature

Superscript

$*$	dimensionless variable

resent works in the fluid mechanics having MHD unsteady flow over thin film with heat and mass transfers.

The aim of the present study is to assume, the case of an unsteady thin film flow under the influence of variable viscosity and thermal conductivity along with the effect of magnetic field. Variable viscosity and thermal conductivity are both considered linear functions of temperature while the surface tension varies quadratically with temperature. The model non-linear partial differential equations are transformed to third and second order ODEs for momentum and energy equations respectively. Resultant equations are solved analytically by HAM and numerically by shooting method. The effects of various parameters such as viscosity, thermal conductivity, thermocapillary number, prandtl number, fluid thickness, Hartmann number and unsteady parameter on the flow and heat transfer have been shown graphically and in tabulated form.

Problem formulation

Governing equations

In a non rotating reference frame thin elastic sheet that emerges from a narrow slit at the origin of the Cartesian coordinate system. The x-axis is considered along the stretching sheet while, the transverse magnetic field $B = B_0/(1-\alpha t)^{1/2}$ is normal to the stretching sheet is applied along the direction of gravity which is located along y-axis. An infinite horizontal disk is placed at z = 0 in a viscous incompressible viscoelastic fluid. Navier-Stokes and energy equations governing the unsteady incompressible flow of a viscoelastic fluid are

$$\frac{\partial u}{\partial x}+\frac{\partial v}{\partial y}=0, \tag{1}$$

$$\rho\left(\frac{\partial u}{\partial t}+u\frac{\partial u}{\partial x}+v\frac{\partial u}{\partial y}\right)=2\frac{\partial}{\partial x}\left(\mu\frac{\partial u}{\partial x}\right)+\frac{\partial}{\partial y}\left(\mu\left(\frac{\partial u}{\partial y}+\frac{\partial v}{\partial x}\right)\right)-\hat{\sigma}B^2u, \tag{2}$$

$$\rho\left(\frac{\partial v}{\partial t}+u\frac{\partial v}{\partial x}+v\frac{\partial v}{\partial y}\right)=\frac{\partial}{\partial x}\left(\mu\left(\frac{\partial u}{\partial y}+\frac{\partial v}{\partial x}\right)\right)+2\frac{\partial}{\partial y}\left(\mu\left(\frac{\partial v}{\partial y}\right)\right), \tag{3}$$

$$\rho C_p\left(\frac{\partial T}{\partial t}+u\frac{\partial T}{\partial x}+v\frac{\partial T}{\partial y}\right)=\frac{\partial}{\partial x}\left(\kappa\frac{\partial T}{\partial x}\right)+\frac{\partial}{\partial y}\left(\kappa\frac{\partial T}{\partial y}\right). \tag{4}$$

To obtain dimensionless form of the Eqs. (1)–(4) with boundary conditions, we introduce the following scaling

$$x=Lx^*,\quad y=\hat{\delta}y^*,\quad u=Uu^*,\quad v=\frac{U\hat{\delta}}{L}v^*,\quad t=\frac{L}{U}t^*,$$
$$T=T^*(T_s-T_0)+T_0, \tag{5}$$

where $\hat{\delta}$ is the vertical length scale, L is horizontal length scale, $\frac{\hat{\delta}}{L}\ll 1$ is aspect ratio, T_0 temperature of fluid at the surface of the stretching sheet and T_s is the temperature of fluid at the surface. By making use of Eq. (5) in Eqs. (1)–(4), after dropping the asterisk we arrive at the following form

$$\frac{\partial u}{\partial x}+\frac{\partial v}{\partial y}=0, \tag{6}$$

$$\rho\left(\frac{\partial u}{\partial t}+u\frac{\partial u}{\partial x}+v\frac{\partial u}{\partial y}\right)=\frac{\partial}{\partial y}\left(\mu\frac{\partial u}{\partial y}\right)-\frac{L\hat{\sigma}B^2}{U}u, \tag{7}$$

$$\rho C_p\left(\frac{\partial T}{\partial t}+u\frac{\partial T}{\partial x}+v\frac{\partial T}{\partial y}\right)=\frac{\partial}{\partial y}\left(\kappa\frac{\partial T}{\partial y}\right), \tag{8}$$

and the boundary conditions [10] are

$$u = U_s, \quad v = 0, \quad T = T_s \ at \ y = 0, \tag{9}$$

$$\mu\frac{\partial u}{\partial y} = \frac{\partial \sigma}{\partial x}, \quad \frac{\partial T}{\partial y} = 0, \quad v = \frac{dh}{dt} \ at \ y = h, \tag{10}$$

where u and v are velocity components along x and y respectively, T is for temperature, $\hat{\sigma}$ represents the electrical conductivity, t denotes time, ν use for kinematic viscosity, ρ express density, liquid film thickness is $h(t)$, μ is variable viscosity, κ is variable thermal conductivity and σ is the surface tension which varies quadratically with temperature

$$\sigma = \sigma_0\left[1 - \frac{h_1(T - T_0)}{2}\right]\frac{\delta(T_0 - T)}{2\nu_0(1 - \alpha t)^{\frac{1}{2}}}, \tag{11}$$

where h_1 and δ represents positive constants. Surface stretching velocity is considered as

$$U_s = \frac{\alpha}{2}x(1 - \alpha t)^{-1}, \tag{12}$$

where α is positive constant. It is assumed that the liquid film surface is smooth and their is no wave. As taken by Liu et al. [7] in 2008, for making uniform film thickness the stretching surface velocity will be independent on the position, shown in Eq. (12). The flow of a non planar thin liquid film first considered by Dandapat [14,15] in 2006 and suggested the notation $h(t)$ as a film thickness of an unsteady stretching sheet. Surface temperature of the stretching sheet are selected as

$$T_s = T_0 - T_{ref}\frac{\alpha^2 x^2}{2(1 - \alpha t)}, \tag{13}$$

where T_0 is the stretching sheet temperature and T_{ref} is reference temperature (constant) for all $t < 1/\alpha$.

Similarity transformation

For transformation purpose the following transformation are used for velocity components

$$u = \frac{\alpha x}{2(1 - \alpha t)}f'(\eta), \tag{14}$$

$$v = -\frac{\alpha}{2}\frac{(\nu_0/b)^{\frac{1}{2}}}{(1 - \alpha t)^{\frac{1}{2}}}\beta f(\eta), \tag{15}$$

where b is Initial stretching rate which is a non-negative constant, while the effective stretching rate is denoted by $b/(1 - \alpha t)$. The temperature function is considered as

$$T = T_0 - T_{ref}\frac{\alpha^2 x^2}{2}(1 - \alpha t)^{-1}\theta(\eta), \tag{16}$$

where η represents similarity variable [5,16] and is defined as

$$\eta = \left(\frac{b}{\nu_0}\right)^{\frac{1}{2}}(1 - \alpha t)^{\frac{-1}{2}}\beta^{-1}y, \tag{17}$$

here β is a constant representing the dimensionless film thickness [5,16]

$$\beta = \left(\frac{b}{\nu_0}\right)^{\frac{1}{2}}(1 - \alpha t)^{\frac{-1}{2}}h(t), \tag{18}$$

here μ is the variable viscosity and κ is the variable thermal conductivity are assumed to vary as a linear function of temperature and defined as

$$\mu = \mu_0[1 + A\theta], \tag{19}$$

$$\kappa = \kappa_0[1 + N\theta], \tag{20}$$

here μ_0 and κ_0 are the viscosity and thermal conductivity respectively, h_1, h_2 are constants, where $A = h_1(T_0 - T_s)$ and $N = h_2(T_0 - T_s)$ are the temperature differences named as viscosity and thermal conductivity parameters respectively. The available data given in Eqs. (11)–(20) are used in the set of Eqs. (6)–(10), we obtain the following

$$(1 + A\theta)f''' + A\theta' f'' - \frac{\Upsilon}{2}[S(\eta f'' + f'^2 - ff'' + 2f') + Maf'] = 0, \tag{21}$$

$$(1 + N\theta)\theta'' + N\theta'^2 - \frac{S\Upsilon}{2}Pr[2\theta + \eta\theta' + 2\theta f' - \theta' f] = 0, \tag{22}$$

with the boundary conditions

$$f(0) = 0, \quad f'(0) = 1, \quad \theta(0) = 1, \tag{23}$$

$$f(1) = 1, \quad f''(1) = M\theta(1), \quad \theta'(1) = 0, \tag{24}$$

where prime represents the differentiation with respect to η, $\Upsilon = \beta^2$ is the non-dimensional film thickness, $S = \alpha/b$ is non-dimensional parameter of unsteadiness, $Ma = L\hat{\sigma}B_0^2/U\rho b$ is Hartmann number, $Pr = \frac{\mu_0 C_p}{\kappa_0}$ is prandtl number and M is the thermocapillary number defined by

$$M = \frac{\delta\sigma_0\alpha T_{ref}\beta}{\mu_0\sqrt{b\nu_0}}.$$

Problem approach

Nusselt number and Skin friction coefficient

The physical quantities of interest are local Nusselt number and the skin friction coefficient which are expressed as.

$$Nu_\chi = \frac{\chi q_w}{\kappa T_{ref}}, \quad C_f = \frac{\tau_w}{\rho U^2/2}, \text{ respectively,}$$

where heat transfer from the sheet q_w and the skin friction τ_w are given by

$$q_w = -\kappa\left(\frac{\partial T}{\partial y}\right)_{y=0}, \quad \tau_w = \mu\left(\frac{\partial u}{\partial y}\right)_{y=0}$$

with κ and μ being variable thermal conductivity and variable viscosity respectively. By making use of transformations (14)–(20) the rate of heat transfer and the skin friction for thin liquid film are reduced to coupled equations

$$Nu_\chi \equiv \frac{2U_s\sqrt{b\nu_0}}{\beta}\theta'(0)Re_\chi, \tag{25}$$

$$C_f \equiv \frac{2^{\frac{3}{2}}(1 + A\theta)}{S\beta}f''(0)Re_\chi^{-1}, \tag{26}$$

where $Re_\chi = U_s\chi/\nu$ is the local Reynolds number.

Solution approach

The model given in Eqs. (21)–(24), are solved by HAM [17]. The functions $f(\eta)$ and $\theta(\eta)$ can be written in term of $\{\eta^m | m = 0, 1, 2, \ldots\}$ as

$$f(\eta) = \sum_{m=0}^{+\infty} a_m \eta^m, \tag{27}$$

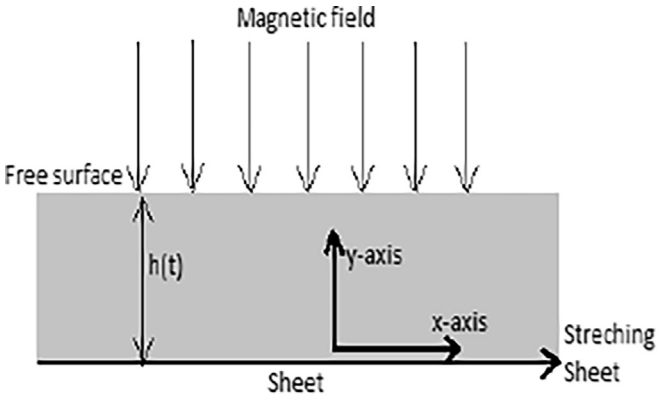

Fig. 1. Geometry of the problem.

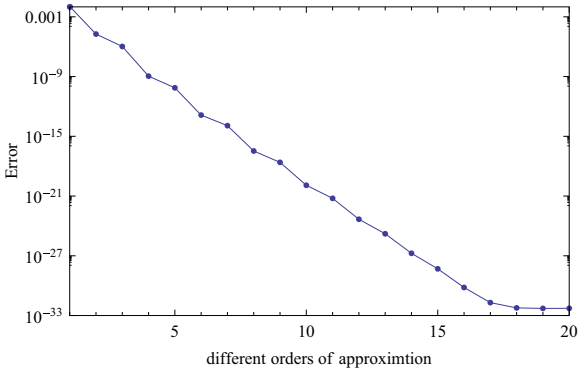

Fig. 2. $A = 0.3$, $N = 0.2$ $S = 0.4$, $Ma = 1$, $M = 1$, $\Upsilon = 0.127013$, $Pr = 1$.

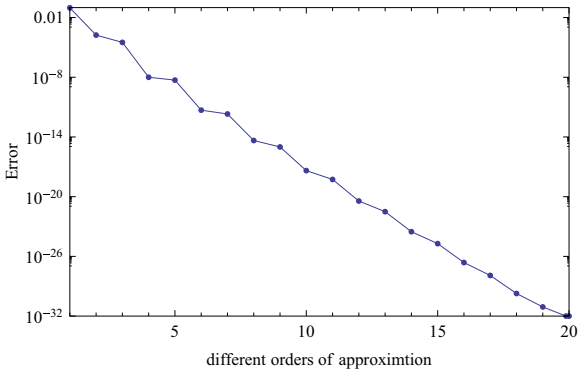

Fig. 3. $A = 0.9$, $N = 0.2$ $S = 0.4$, $Ma = 1$, $M = 1$, $\Upsilon = 0.127013$, $Pr = 1$.

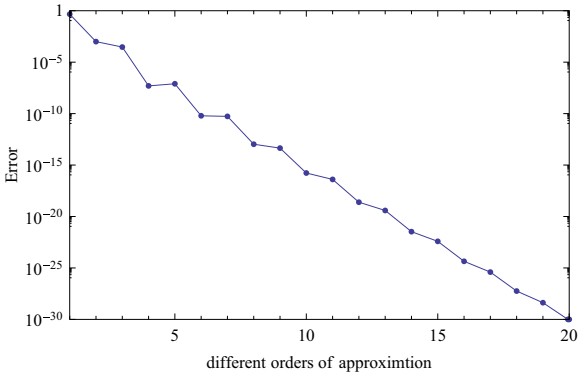

Fig. 4. $A = 2.0$, $N = 0.2$ $S = 0.4$, $Ma = 1$, $M = 1$, $\Upsilon = 0.127013$, $Pr = 1$.

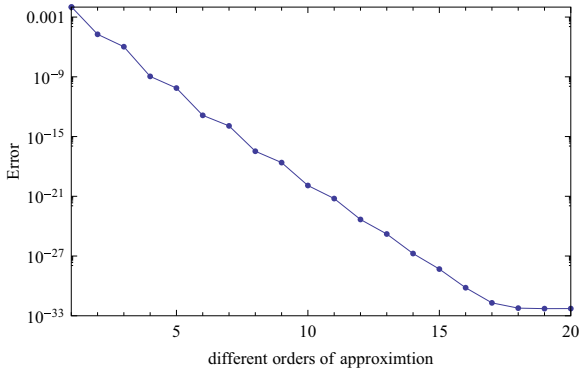

Fig. 5. $N = 0.2$, $A = 0.3$, $S = 0.4$, $Ma = 1$, $M = 1$, $\Upsilon = 0.127013$, $Pr = 1$.

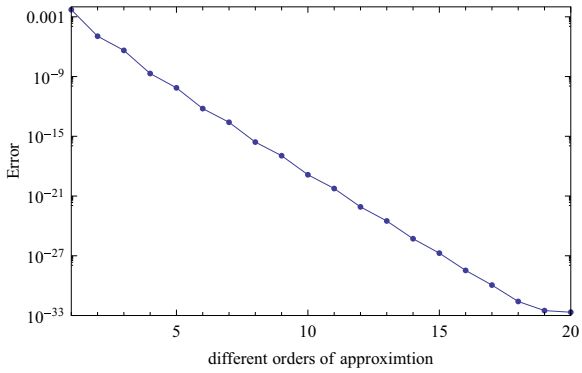

Fig. 6. $N = 0.8$, $A = 0.3$, $S = 0.4$, $Ma = 1$, $M = 1$, $\Upsilon = 0.127013$, $Pr = 1$.

$$\theta(\eta) = \sum_{m=0}^{+\infty} c_m \eta^m, \tag{28}$$

where a_m and c_m are the constants. The initial guesses for the corresponding $f(\eta)$ and $\theta(\eta)$ satisfying the given boundary conditions (23) and (24) are

$$f_0(\eta) = \eta - \frac{M\theta_0(\eta)}{4}\eta^2 + \frac{M\theta_0(\eta)}{4}\eta^3, \tag{29}$$

$$\theta_0(\eta) = 1. \tag{30}$$

where the auxiliary linear operators for Eqs. (29) and (30) are $\pounds_f = \partial^4/\partial\eta^4$ and $\pounds_\theta = \partial^2/\partial\eta^2$, respectively with the characteristics

$$\pounds_f[C_1 + C_2\eta + C_3\eta^2 + C_4\eta^3] = 0, \tag{31}$$

$$\pounds_\theta[C_1 + C_2\eta] = 0, \tag{32}$$

the integration constants are denoted by C_1, C_2, C_3 and C_4. The nonlinear operators are constructed from of Eqs. (21) and (22) as

$$\aleph_f[F(\eta;q), \Theta(\eta;q), \Gamma(q)] = (1 + A\Theta)F''' + A\Theta'F'' - \frac{S\Gamma}{2}[\eta F'' + F'^2 - FF'' + 2(1 + Ma)F'], \tag{33}$$

$$\aleph_\theta[F(\eta;q), \Theta(\eta;q), \Gamma(q)] = (1 + N\Theta)\Theta'' + N\Theta'^2 - \frac{S\Gamma}{2}Pr[2\Theta + \eta\Theta' + 2\Theta F' - \Theta' F], \tag{34}$$

where the unknown functions $F(\eta;q)$ and $\Theta(\eta;q)$ depends upon η and q, and the function Γ dependents only on q. Prime in the superscript indicates the number of derivatives with respect to η. Here auxiliary parameters are $\hbar_f \neq 0$ and $\hbar_\theta \neq 0$, while the non-zero

Table 1
Optimal value of convergence control parameters versus different orders of approximation.

Order of approximation	h_f	h_θ	ε_m^t	CPU time
2	−0.758911	−0.774441	3.32135×10^{-6}	12.8339 s
3	−0.728282	−0.748189	6.82839×10^{-7}	19.5611 s
4	−0.771597	−0.790182	$1.10068 \times 10^{-}9$	36.4740 s
5	−0.761503	−0.794459	7.04277×10^{-11}	64.1040 s
6	−0.768268	−0.793531	1.96473×10^{-13}	110.015 s

Table 2
Individual averaged squared residual errors using optimal values of auxiliary parameters.

m	ε_m^f	ε_m^θ
2	2.81278×10^{-6}	2.76509×10^{-7}
4	1.44400×10^{-10}	3.90453×10^{-11}
6	1.60377×10^{-14}	6.42270×10^{-15}
8	4.08680×10^{-18}	1.48394×10^{-18}
10	1.61538×10^{-21}	4.01104×10^{-22}
16	9.68642×10^{-32}	1.24820×10^{-32}
20	6.68298×10^{-34}	2.11852×10^{-34}
26	6.72872×10^{-34}	2.11852×10^{-34}
30	6.72872×10^{-34}	2.11852×10^{-34}
40	6.72872×10^{-34}	2.11852×10^{-34}

Table 3
Convergence of HAM on the basis of skin friction $f''(0)$ and heat flux $-\theta'(0)$ for selected values of $A = 0.3$, $N = 0.2$, $S = 0.4$, $Ma = 1$, $M = 1$, $\Upsilon = 0.127013$, $Pr = 1$.

m	$f''(0)$	$-\theta'(0)$
1	−0.47645821694706656707	0.08029071840320629929
5	−0.47296390059640400496	0.08228968461130221429
10	−0.47296378115567143773	0.08228961268275264755
15	−0.47296378115446224487	0.08228961268191567756
20	−0.47296378115446220151	0.08228961268191566292
25	−0.47296378115446220151	0.08228961268191566292
30	−0.47296378115446220151	0.08228961268191566292
35	−0.47296378115446220151	0.08228961268191566292
40	−0.47296378115446220151	0.08228961268191566292

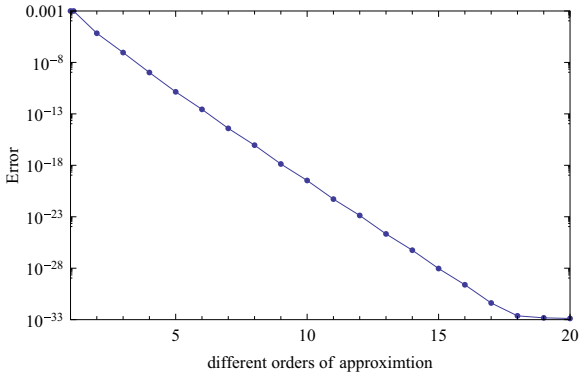

Fig. 7. $N = 2.0$, $A = 0.3$, $S = 0.4$, $Ma = 1$, $M = 1$, $\Upsilon = 0.127013$, $Pr = 1$.

auxiliary functions are represented by H_f and H_θ. Deformation equation for zeroth order can be expressed as

$$(1-q)\pounds_f[F(\eta,q) - f_0(\eta)] = q\hbar_f H_f \aleph_f[F(\eta,q), \Theta(\eta,q), \Gamma(q)], \tag{35}$$

$$(1-q)\pounds_\theta[\Theta(\eta,q) - \theta_0(\eta)] = q\hbar_\theta H_\theta \aleph_\theta[F(\eta,q), \Theta(\eta,q), \Gamma(q)], \tag{36}$$

the boundary conditions are

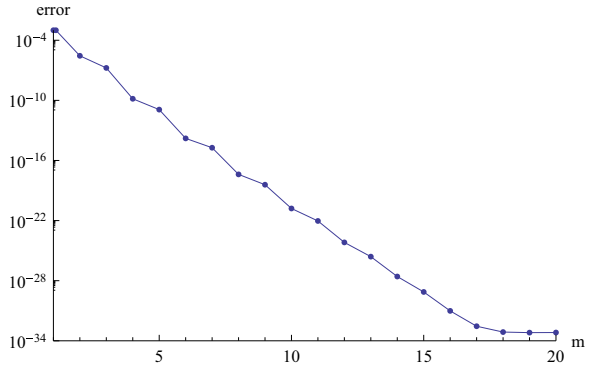

Fig. 8. Error of Azimuthal velocity f at 20th-order HAM via *Mathematica* package **BVPh2.0** approximation, where $A = 0.3$, $N = 0.2$ $S = 0.4$, $Ma = 1$, $M = 1$, $\Upsilon = 0.127013$, $Pr = 1$.

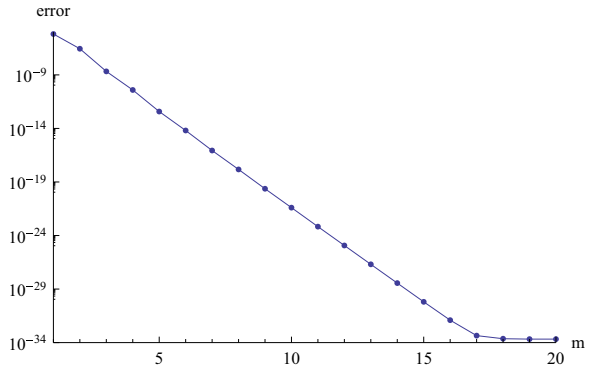

Fig. 9. Error of temperature θ at 20th-order HAM via *Mathematica* package **BVPh2.0** approximation, where $A = 0.3$, $N = 0.2$ $S = 0.4$, $Ma = 1$, $M = 1$, $\Upsilon = 0.127013$, $Pr = 1$.

$$F(0;q) = 0, \quad F'(0;q) = 1, \quad \Theta(0;q) = 1, \quad F(1;q) = 1,$$
$$F''(1;q) = M\Theta(1;q), \quad \Theta'(1;q) = 0, \tag{37}$$

the embedding parameter is $0 \leqslant q \leqslant 1$. From Eqs. (35) and (36), it is observed that when, $q = 0$, implies that equations (29) and (30) are obtained as

$$F(\eta;0) = f_0(\eta), \quad \Theta(\eta;0) = \theta_0(\eta). \tag{38}$$

As $q = 1$ and $\hbar_f, \hbar_\theta \neq 0$ and $H_f, H_\theta \neq 0$, then equations (35)–(37) gives equations (21)–(24), respectively, but

$$F(\eta;1) = f(\eta), \quad \Theta(\eta;1) = \theta(\eta), \quad \Gamma(1) = \Upsilon. \tag{39}$$

On increasing q from zero to one, the approximate solutions $F(\eta;q)$ and $\Theta(\eta;q)$ converges to exact solutions $f(\eta)$ and $\theta(\eta)$ respectively.

$$\Gamma(0) = \Upsilon_0, \tag{40}$$

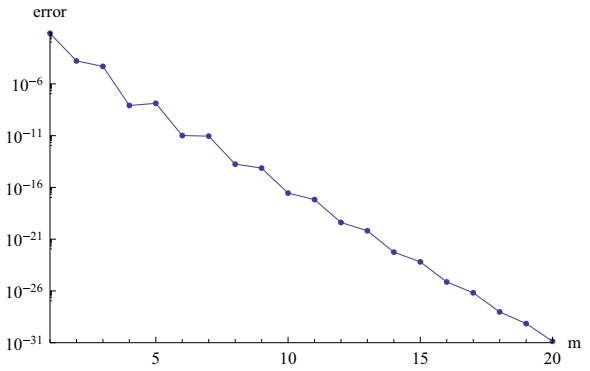

Fig. 10. Error of Azimuthal velocity f at 20th-order HAM via *Mathematica* package **BVPh2.0** approximation, where $A = 2.0$, $N = 0.2$ $S = 0.4$, $Ma = 1$, $M = 1$, $\Upsilon = 0.127013$, $Pr = 1$.

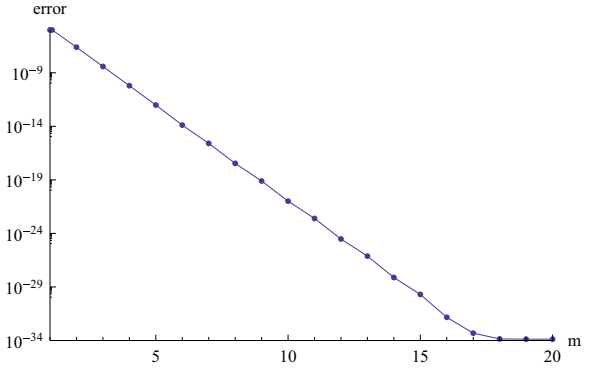

Fig. 11. Error of temperature θ at 20th-order HAM via *Mathematica* package **BVPh2.0** approximation, where $A = 2.0$, $N = 0.2$ $S = 0.4$, $Ma = 1$, $M = 1$, $\Upsilon = 0.127013$, $Pr = 1$.

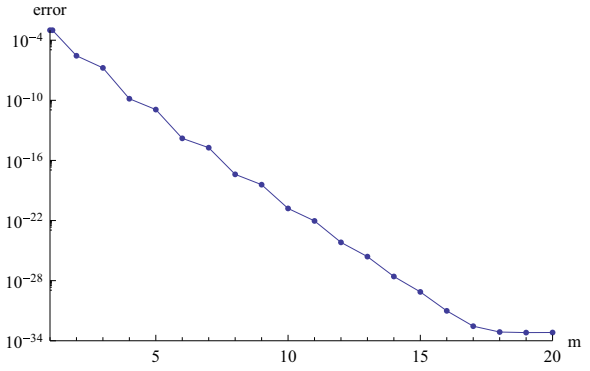

Fig. 12. Error of Azimuthal velocity f at 20th-order HAM via *Mathematica* package **BVPh2.0** approximation, where $N = 0.2$, $A = 0.3$, $S = 0.4$, $Ma = 1$, $M = 1$, $\Upsilon = 0.127013$, $Pr = 1$.

initial guess to the time-scale parameter Υ. By using Maclaurin series combining with (29) and (30), the functions $F(\eta;q)$, $\Theta(\eta;q)$ and $\Gamma(q)$ can be expand as a series of q as

$$F(\eta;q) = f_0(\eta) + \sum_{m=1}^{+\infty} f_m(\eta) q^m, \tag{41}$$

$$\Theta(\eta;q) = \theta_0(\eta) + \sum_{m=1}^{+\infty} \theta_m(\eta) q^m, \tag{42}$$

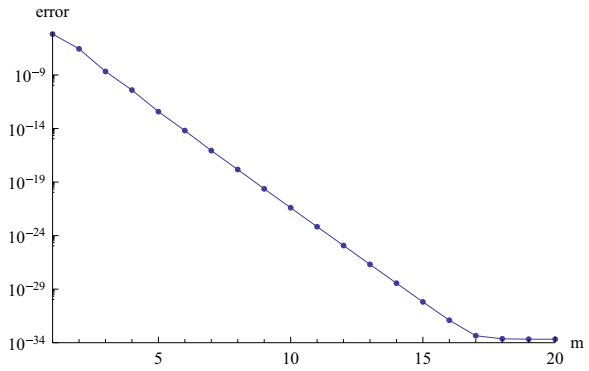

Fig. 13. Error of temperature θ at 20th-order HAM via *Mathematica* package **BVPh2.0** approximation, where $N = 0.2$, $A = 0.3$, $S = 0.4$, $Ma = 1$, $M = 1$, $\Upsilon = 0.127013$, $Pr = 1$.

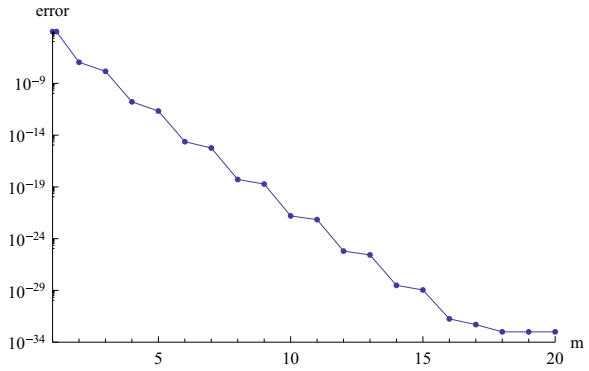

Fig. 14. Error of Azimuthal velocity f at 20th-order HAM via *Mathematica* package **BVPh2.0** approximation, where $N = 2.0$, $A = 0.3$, $S = 0.4$, $Ma = 1$, $M = 1$, $\Upsilon = 0.127013$, $Pr = 1$.

$$\Gamma(q) = \Upsilon_0 + \sum_{m=1}^{+\infty} \Upsilon_m q^m, \tag{43}$$

where

$$f_m(\eta) = \frac{1}{m!}\left[\frac{\partial^m F(\eta;q)}{\partial q^m}\right]_{q=0}, \tag{44}$$

$$\theta_m(\eta) = \frac{1}{m!}\left[\frac{\partial^m \Theta(\eta;q)}{\partial q^m}\right]_{q=0}, \tag{45}$$

$$\Upsilon_m = \frac{1}{m!}\left[\frac{\partial^m \Gamma(q)}{\partial q^m}\right]_{q=0}, \tag{46}$$

using (39) we have

$$f(\eta) = f_0(\eta) + \sum_{m=1}^{+\infty} f_m(\eta), \tag{47}$$

$$\theta(\eta) = \theta_0(\eta) + \sum_{m=1}^{+\infty} \theta_m(\eta), \tag{48}$$

$$\Upsilon = \Upsilon_0 + \sum_{m=1}^{+\infty} \Upsilon_m, \tag{49}$$

Differentiating m-times Eqs. (35) and (36) with respect to q after putting $q = 0$ and dividing both sides by $m!$, finally we get mth-order deformation equations

Table 4
Variation of $\beta = \Upsilon^{\frac{1}{2}}$, $f''(0)$, $\theta(1)$ and $-\theta'(0)$ using 20th-order HAM via *Mathematica* package **BVPh2.0** approximation when $S = 0.4$, $Ma = 1$, $M = 1$, $Pr = 1$.

h_f	h_θ	β	$f''(0)$	$\theta(1)$	$-\theta'(0)$
$A = 0.3, N = 0.2$					
−0.251187	−0.310346	2.82701	−0.0541125	0.177935	2.20751
−0.279832	−0.336978	2.62701	−0.0675005	0.211480	2.03789
−0.310190	−0.365617	2.42701	−0.0840230	0.250869	1.86531
$A = 3.0, N = 0.2$					
−0.0853798	−0.622798	1.62701	−0.160536	0.479593	1.137740
−0.2178240	−0.511561	1.42701	−0.200722	0.555329	0.947237
−0.1231730	−0.271671	1.22701	−0.247608	0.636693	0.756662
$N = 0.2, A = 0.3$					
−0.251187	−0.310346	2.82701	−0.0541125	0.177935	2.20751
−0.279832	−0.336978	2.62701	−0.0675005	0.211480	2.03789
−0.310190	−0.365617	2.42701	−0.0840230	0.250869	1.86531
$N = 2.0, A = 0.3$					
−0.550077	−0.264362	1.62701	−0.295292	0.701737	0.565891
−0.586416	−0.277023	1.42701	−0.332292	0.760543	0.456357
−0.623966	−0.289294	1.22701	−0.368829	0.816176	0.352173

Table 5
Comparison of the values of $\beta = \Upsilon^{\frac{1}{2}}$, $f''(0)$, $\theta(1)$ and $-\theta'(0)$ using 20th-order HAM via *Mathematica* package **BVPh2.0** approximation and Shooting method for the case $N = 0.2, S = 0.4, Ma = 1, M = 1, Pr = 1$ and several values of A.

A	HAM				Shooting method			
	β	$f''(0)$	$\theta(1)$	$-\theta'(0)$	β	$f''(0)$	$\theta(1)$	$-\theta'(0)$
0.3	2.927010	−0.0484233	0.163124	2.29138	2.927010	−0.0484143	0.163111	2.29141
0.9	2.627010	−0.0587333	0.211482	2.03809	2.627010	−0.0587318	0.211483	2.03809
1.5	2.327010	−0.0767967	0.273006	1.77807	2.327010	−0.0766745	0.273006	1.77809
2.0	2.162701	−0.0892719	0.313156	1.63225	2.162701	−0.0892711	0.313156	1.63224
3.0	1.827010	−0.1270170	0.410961	1.32567	1.827010	−0.1270160	0.410960	1.32567
4.0	1.527010	−0.1761900	0.516684	1.04249	1.527010	−0.1763600	0.516637	1.04273

Table 6
Comparison of the values of $\beta = \Upsilon^{\frac{1}{2}}$, $f''(0)$, $\theta(1)$ and $-\theta'(0)$ using 20th-order HAM via *Mathematica* package **BVPh2.0** approximation and Shooting method for the case $A = 0.3$, $S = 0.4$, $Ma = 1$, $M = 1$, $Pr = 1$ and several values of N.

N	HAM				Shooting method			
	β	$f''(0)$	$\theta(1)$	$-\theta'(0)$	β	$f''(0)$	$\theta(1)$	$-\theta'(0)$
0.2	2.927010	−0.0484233	0.163124	2.291380	2.927010	−0.0484143	0.163111	2.291410
0.8	2.627010	−0.0913319	0.281077	1.563790	2.627010	−0.0913320	0.281077	1.563780
1.4	2.327010	−0.1524810	0.428876	1.118070	2.327010	−0.1524780	0.428860	1.118070
2.0	2.162701	−0.2025740	0.540546	0.867892	2.162701	−0.2025720	0.540541	0.867893
2.6	1.827010	−0.2799380	0.686979	0.587800	1.827010	−0.2799380	0.686979	0.587800
3.0	1.527010	−0.3417560	0.788387	0.400645	1.527010	−0.3417560	0.788386	0.400645

Table 7
Comparison of the values of $\beta = \Upsilon^{\frac{1}{2}}$, $f''(0)$, $\theta(1)$ and $-\theta'(0)$ using 20th-order HAM via *Mathematica* package **BVPh2.0** approximation and Shooting method for the case $A = 0.3$, $S = 0.4$, $Ma = 1$, $M = 1$, $N = 0.2$ and several values of Pr.

Pr	HAM				Shooting method			
	β	$f''(0)$	$\theta(1)$	$-\theta'(0)$	β	$f''(0)$	$\theta(1)$	$-\theta'(0)$
0.7	2.927010	−0.0746875	0.2462840	1.88479	2.927010	−0.0746869	0.2462830	1.88478
1.0	2.627010	−0.0675005	0.2114800	2.03789	2.627010	−0.0674985	0.2114770	2.03789
2.0	2.327010	−0.0391912	0.1186500	2.59173	2.327010	−0.0391646	0.1185800	2.59190
3.0	2.162701	−0.0268261	0.0795568	2.96080	2.162701	−0.0267296	0.0793403	2.96179
4.0	1.827010	−0.0309070	0.0862517	2.88660	1.827010	−0.0308063	0.0860676	2.88733
5.0	1.527010	−0.0401968	0.1064570	2.69223	1.527010	−0.0400971	0.1063520	2.69253

Table 8
Comparison of the values of $\beta = \Upsilon^{1}_{2}$, $f''(0)$, $\theta(1)$ and $-\theta'(0)$ using 20th-order HAM via *Mathematica* package **BVPh2.0** approximation and Shooting method for the case $A = 0.3$, $Pr = 1$, $Ma = 1$, $M = 1$, $N = 0.2$ and several values of S.

S	HAM				Shooting method			
	β	$f''(0)$	$\theta(1)$	$-\theta'(0)$	β	$f''(0)$	$\theta(1)$	$-\theta'(0)$
0.4	3.927011	−0.015990	0.067813	3.10660	3.927011	−0.015803	0.067561	3.10843
0.6	3.627012	−0.009325	0.043286	3.51408	3.627012	−0.008893	0.042722	3.52120
0.8	3.327013	−0.007229	0.034558	3.71846	3.327013	−0.006643	0.033795	3.73098
1.0	3.162704	−0.005545	0.026966	3.94455	3.162704	−0.004758	0.025803	3.97183
1.2	2.827015	−0.006073	0.029408	3.86538	2.827015	−0.005376	0.028490	3.88348
1.4	2.527016	−0.007079	0.033905	3.73582	2.527016	−0.006479	0.033124	3.74892

Table 9
Comparison of the values of $\beta = \Upsilon^{1}_{2}$, $f''(0)$, $\theta(1)$ and $-\theta'(0)$ using 20th-order HAM via *Mathematica* package **BVPh2.0** approximation and Shooting method for the case $A = 0.3$, $Pr = 1$, $S = 0.4$, $M = 1$, $N = 0.2$ and several values of Ma.

Ma	HAM				Shooting method			
	β	$f''(0)$	$\theta(1)$	$-\theta'(0)$	β	$f''(0)$	$\theta(1)$	$-\theta'(0)$
0.0	3.927011	−0.0185688	0.067840	3.10639	3.927011	−0.0184003	0.067562	3.10818
1.0	3.627012	−0.0222134	0.088280	2.86562	3.627012	−0.0221169	0.088147	2.86630
3.0	3.327013	−0.0253259	0.114932	2.62232	3.327013	−0.0252883	0.114886	2.62254
5.0	3.162704	−0.0263906	0.132768	2.48782	3.162704	−0.0263731	0.132749	2.48793
7.0	2.827015	−0.0354123	0.177984	2.20882	2.827015	−0.0354088	0.177981	2.20883
10	2.527016	−0.0451973	0.230535	1.95381	2.527016	−0.0451969	0.230535	1.95381

Table 10
Comparison of the values of $\beta = \Upsilon^{1}_{2}$, $f''(0)$, $\theta(1)$ and $-\theta'(0)$ using 20th-order HAM via *Mathematica* package **BVPh2.0** approximation and Shooting method for the case $A = 0.3$, $Pr = 1$, $S = 0.4$, $Ma = 1$, $N = 0.2$ and several values of M.

M	HAM				Shooting method			
	β	$f''(0)$	$\theta(1)$	$-\theta'(0)$	β	$f''(0)$	$\theta(1)$	$-\theta'(0)$
0.0	1.927013	0.000000	0.380657	1.422660	1.927013	0.000001	0.380650	1.422691
0.3	1.627014	−0.058208	0.480758	1.140650	1.627014	−0.058208	0.480758	1.140647
0.5	1.327015	−0.128089	0.596573	0.853361	1.327015	−0.128088	0.596573	0.853361
0.7	1.127016	−0.212034	0.679354	0.663376	1.127016	−0.212033	0.679354	0.663375
1.0	0.827017	−0.376263	0.803434	0.395479	0.827017	−0.376262	0.803434	0.395480
1.2	0.527018	−0.532011	0.911731	0.174125	0.527018	−0.532010	0.911730	0.174125

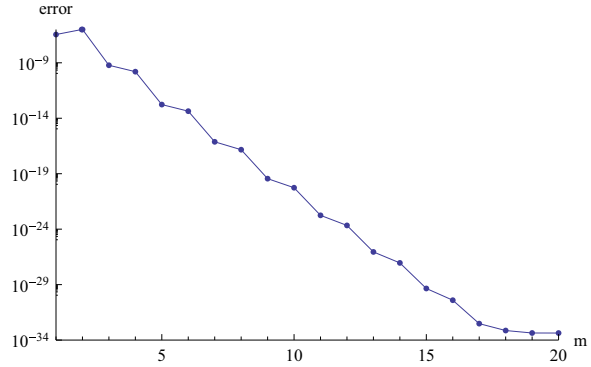

Fig. 15. Error of temperature θ at 20th-order HAM via *Mathematica* package **BVPh2.0** approximation, where $N = 2.0$, $A = 0.3$, $S = 0.4$, $Ma = 1$, $M = 1$, $\Upsilon = 0.127013$, $Pr = 1$.

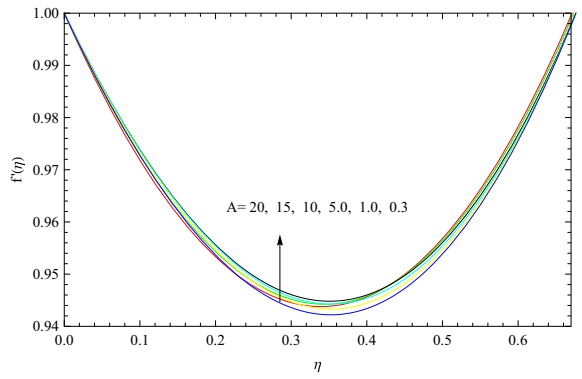

Fig. 16. The effect of A on velocity profile with $N = 0.2$, $M = 1$, $Ma = 1$, $Pr = 1$, $S = 0.4$, $\Upsilon = 1.027013$.

$$\pounds_f[f_m(\eta) - \chi_m f_{m-1}(\eta)] = \hbar_f H_f(\eta) R_{f,m}(\eta), \tag{50}$$

$$\pounds_\theta[\theta_m(\eta) - \chi_m \theta_{m-1}(\eta)] = \hbar_\theta H_\theta(\eta) R_{\theta,m}(\eta), \tag{51}$$

with boundary conditions

$$f_m(0) = 0, \quad f'_m(0) - 1 = 0, \quad \theta_m(0) - 1 = 0, \tag{52}$$

$$f_m(1) - 1 = 0, \quad f''_m(1) - M\theta_m(1) = 0, \quad \theta'_m(1) = 0, \tag{53}$$

for $m \geqslant 1$

$$R_{f,m}(\eta) = f'''_{m-1} + \sum_{n=0}^{m-1}\Bigg[\Bigg(A\theta_n f'''_{m-1-n} + A\theta'_n f''_{m-1-n} - \frac{S}{2}\eta\Upsilon_n f''_{m-1-n} - 2(1+Ma)\Upsilon_n f'_{m-1-n}\Bigg) + \Upsilon_{m-1-n}\sum_{i=0}^{n}(f_i f''_{n-i} - f'_i f'_{n-i})\Bigg], \tag{54}$$

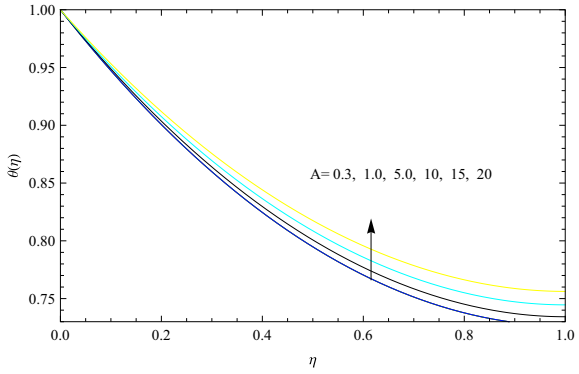

Fig. 17. The effect of A on temperature profile with $N = 0.2$, $M = 1$, $Ma = 1$, $Pr = 1$, $S = 0.4$, $\Upsilon = 1.027013$.

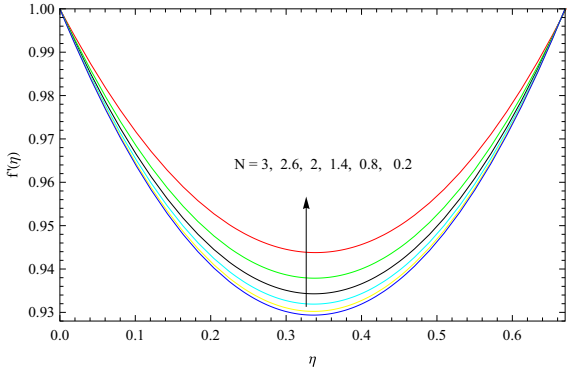

Fig. 18. The effect of N on velocity profile with $A = 0.3$, $M = 1$, $Ma = 1$, $Pr = 1$, $S = 0.4$, $\Upsilon = 1.027013$.

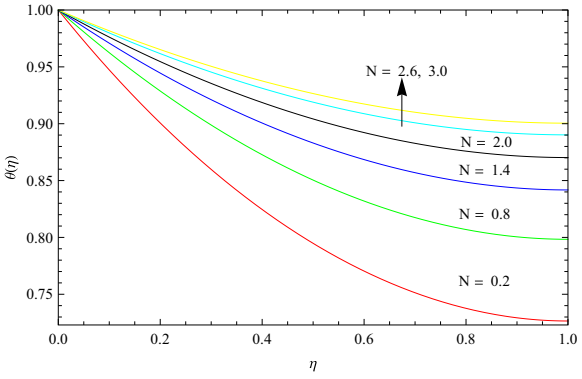

Fig. 19. The effect of N on temperature profile with $A = 0.3$, $M = 1$, $Ma = 1$, $Pr = 1$, $S = 0.4$, $\Upsilon = 1.027013$.

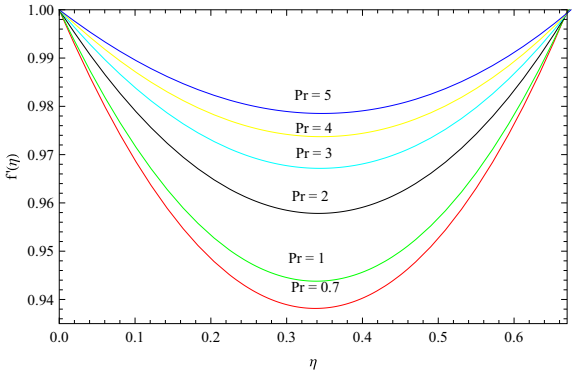

Fig. 20. The effect of Pr on velocity profile with $A = 0.3$, $M = 1$, $Ma = 1$, $N = 0.2$, $S = 0.4$, $\Upsilon = 1.027013$.

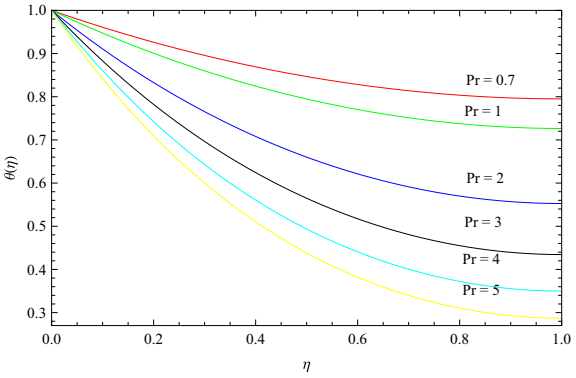

Fig. 21. The effect of Pr on temperature profile with $A = 0.3$, $M = 1$, $Ma = 1$, $N = 0.2$, $S = 0.4$, $\Upsilon = 1.027013$.

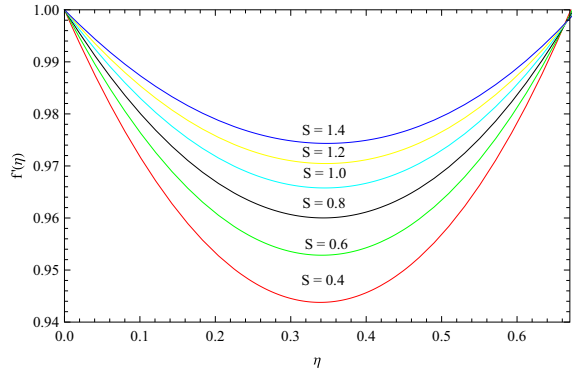

Fig. 22. The effect of S on velocity profile with $A = 0.3$, $M = 1$, $Ma = 1$, $N = 0.2$, $Pr = 1$, $\Upsilon = 1.027013$.

$$R_{\theta,m}(\eta) = \theta''_{m-1} + \sum_{n=0}^{m-1}\Big[N\theta_n\theta''_{m-1-n} + N\theta'_n\theta'_{m-1-n} - SPr(\Upsilon_n\theta_{m-1-n} + \frac{1}{2}\eta\Upsilon_n\theta'_{m-1-n} + \Upsilon_{m-1-n}\sum_{i=0}^{n}(\theta_i f'_{n-i} - \theta'_i f_{n-i})\Big], \tag{55}$$

and

$$\chi_m = \begin{cases} 1, & m > 1, \\ 0, & m = 1, \end{cases}$$

the solution of (50) and (51) can be expressed as

$$f_m(\eta) = \int_0^\eta\int_0^\eta\int_0^\eta\int_0^\eta \hbar_f H_f(s)R_{f,m}(s)dsdsdsds + \chi_m f_{m-1} + C_1 + C_2\eta + C_3\eta^2 + C_4\eta^3, \tag{56}$$

$$\theta_m(\eta) = \int_0^\eta\int_0^\eta \hbar_\theta H_\theta(s)R_{\theta,m}(s)dsds + \chi_m\theta_{m-1} + C_1 + C_2\eta. \tag{57}$$

Thus mth-order approximation of $f(\eta)$, $\theta(\eta)$ and Υ are expressed as

$$f(\eta) \approx \sum_{n=0}^{m} f_n(\eta), \tag{58}$$

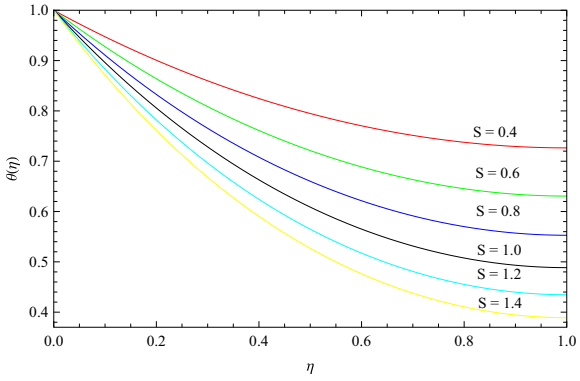

Fig. 23. The effect of S on temperature profile with $A = 0.3$, $M = 1$, $Ma = 1$, $N = 0.2$, $Pr = 1$, $\Upsilon = 1.027013$.

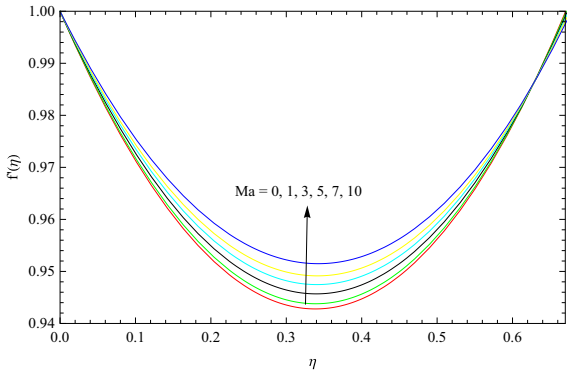

Fig. 24. The effect of Ma on velocity profile with $A = 0.3$, $M = 1$, $S = 0.4$, $N = 0.2$, $Pr = 1$, $\Upsilon = 1.027013$.

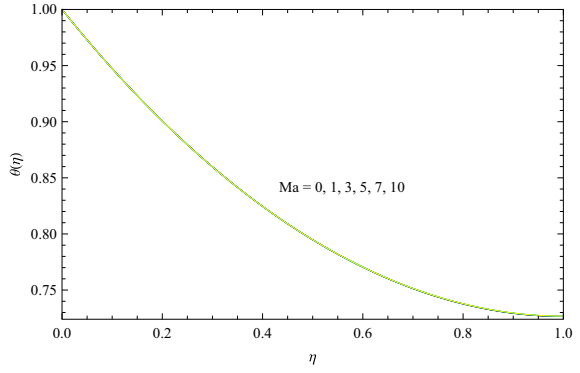

Fig. 25. The effect of Ma on temperature profile with $A = 0.3$, $M = 1$, $S = 0.4$, $N = 0.2$, $Pr = 1$, $\Upsilon = 1.027013$.

$$\theta(\eta) \approx \sum_{n=0}^{m} \theta_n(\eta), \tag{59}$$

$$\Upsilon \approx \sum_{n=0}^{m-1} \Upsilon_n, \tag{60}$$

by simultaneously solving equation $f_{n+1}(\eta)$ with the help of the boundary conditions $f_{n+1}(1) = 0$ and $f''_{n+1}(1) = 0$ mention in (53) $\forall\ n \geqslant 0$ to obtained Υ_n.

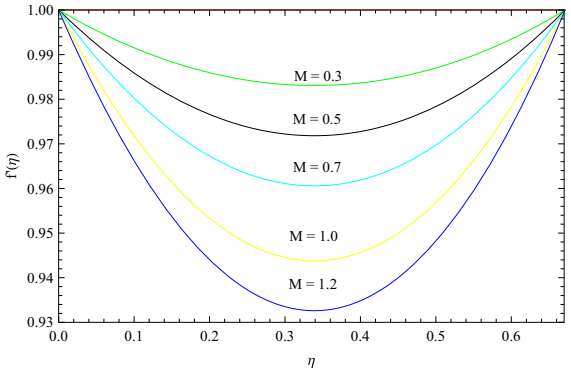

Fig. 26. The effect of M on velocity profile with $A = 0.3$, $Ma = 1$, $S = 0.4$, $N = 0.2$, $Pr = 1$, $\Upsilon = 1.027013$.

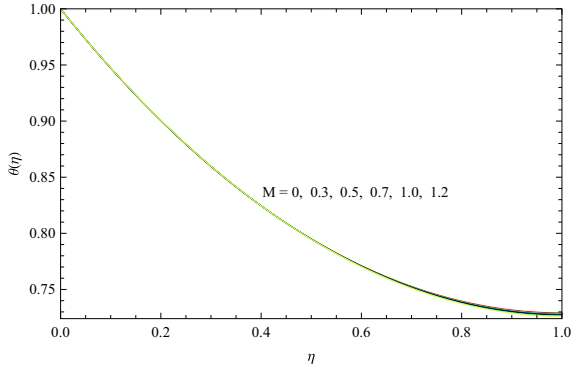

Fig. 27. The effect of M on temperature profile with $A = 0.3$, $Ma = 1$, $S = 0.4$, $N = 0.2$, $Pr = 1$, $\Upsilon = 1.027013$.

Optimal convergence control parameters

First to check the validity of the method we made error analysis before giving physical predictions. For this aim, Figs. 1–6 and Tables 1–3 are made. Minimum error 10^{-40} is fixed in **BVPh2.0** package during solution. Advantage of this method is to determine the solution region and rate of the homotopy series expansions for this the auxiliary parameters $\hbar_f \neq 0$ and $\hbar_\theta \neq 0$ are involve in the solutions (50) and (51). To obtain the optimal values of $\hbar_f$ and $\hbar_\theta$, average residual error introduce by Liao [18] were used as:

$$\varepsilon_m^f = \frac{1}{k+1}\sum_{j=0}^{k}\left[\aleph_f\left(\sum_{i=0}^{m}F(\eta)\sum_{i=0}^{m}\Theta(\eta)\right)_{\eta=j\delta\eta}\right]^2 d\eta, \tag{61}$$

$$\varepsilon_m^\theta = \frac{1}{k+1}\sum_{j=0}^{k}\left[\aleph_\theta\left(\sum_{i=0}^{m}F(\eta)\sum_{i=0}^{m}\Theta(\eta)\right)_{\eta=j\delta\eta}\right]^2 d\eta, \tag{62}$$

Due to Liao [18]

$$\varepsilon_m^t = \varepsilon_m^f + \varepsilon_m^\theta, \tag{63}$$

where ε_m^t is called total squared residual error, $\delta\eta = 0.5$ and $k = 20$. Minimizing total average squared residual error by employing ***Mathematica*** package **BVPh2.0** [19]. To observe error for different order of approximation by varying different parameters, we first varying variable viscosity parameter A and fixing $N = 0.2$ $S = 0.4$, $Ma = 1$, $M = 1$, $\Upsilon = 0.127013$, $Pr = 1$. Figs. 1–3 illustrates the maximum average squared residual error at different orders of approximation. In Fig. 1, for $A = 0.3$ it is observed that as the order of

approximation is increased the total averaged squared residual errors and averaged squared residual errors are getting smaller, also when $A = 0.3$, the error is streakily decreased as compared to the case for $A = 0.9$ and $A = 2.0$ as shown in Figs. 2 and 3 respectively. Similarly different graphs are shown in Figs. 4–6 by varying variable thermal conductivity parameter N fixing $A = 0.3$, $S = 0.4$, $Ma = 1$, $M = 1$, $\Upsilon = 0.127013$ and $Pr = 1$. For $N = 0.2$ the order of approximation is increased the total averaged squared residual errors and averaged squared residual errors are decrease. Similarly errors of Azimuthal velocity f and temperature θ are observed for different values of A in Figs. 7–10 and for different values of N in Figs. 11–14. In addition, Table 1 presents the optimal values of convergence control parameters as well as the minimum values of total averaged squared residual error versus different orders of approximation for the values $A = 0.3$, $N = 0.2$, $S = 0.4$, $Ma = 1$, $M = 1$, $\Upsilon = 0.127013$ and $Pr = 1$. Table 2 displays the individual average squared residual error at different orders of approximations using the self selection of optimal values by ***Mathematica*** package **BVPh2.0** for $A = 0.3$, $N = 0.2$, $S = 0.4$, $Ma = 1$, $M = 1$, $\Upsilon = 0.127013$ and $Pr = 1$. Table 3 shows that twenty Decimal place accuracy take place of $f''(0)$ and twenty decimal place accuracy take place of $-\theta'(0)$ after fifteenth order of approximation.

Results and discussion

As we obtained nonlinear couple of differential Eqs. (21) and (22) subject to the physical boundary conditions (23) and (24), which are analytically solved by using HAM and numerically solved by Shooting method for selected values of variable viscosity parameter, thermal conductivity parameter, Hartmann number, Prandtl number, unsteadiness parameter, thermocapillary number and dimensionless film thickness. Different effects of $\hbar_f$ and $\hbar_\theta$ on $\beta = \Upsilon^{\frac{1}{2}}$, $f''(0)$, $\theta(1)$ and $-\theta'(0)$ is shown in Table 4 using 20th-order HAM approximation when $S = 0.4$, $M = 1$, $Pr = 1$, $Ma = 1$, $N = 0.2$ and $A = 0.3$, 3.0. Similarly in Table 4 we observe different effects for $\hbar_f$ and $\hbar_\theta$ on $\beta = \Upsilon^{\frac{1}{2}}$, $f''(0)$, $\theta(1)$ and $-\theta'(0)$ for $S = 0.4$, $M = 1$, $Pr = 1$, $Ma = 1$, $A = 0.3$ and $N = 0.2, 2.0$. The effects of A, N, Pr, S, Ma and M on β, $f''(0)$, $\theta(1)$ and $-\theta'(0)$ are presented in Tables 5–10. For comparison, we used both HAM and Shooting method to observed and discuss different effects of the physical parameters by varying some parameter while keeping the remaining parameters fixed.

Based on Table 5, when $N = 0.2$, $S = 0.4$, $Ma = 1$, $M = 1$, $Pr = 1$ and increasing the value of variable viscosity parameter A reduce the film thickness $\beta = \Upsilon^{\frac{1}{2}}$ and decrease the skin friction $f''(0)$ and heat flux $-\theta'(0)$, while increases the value of free temperature $\theta(1)$. Same behavior is observed by increasing variable viscosity parameter A and reducing the film thickness we see that up to 4, 5 decimal place accuracy take place in both methods HAM and Shooting as displaced in Table 5. Similar case for increasing thermal conductivity parameter N meaningful impacts in the values of $-\theta'(0)$, $\theta(1)$ and $f''(0)$ is seen. In Table 6, when film thickness is reduced and N is increased where the values of $A = 0.3$, $S = 0.4$, $Ma = 1$, $M = 1$ and $Pr = 1$ then the skin friction $f''(0)$ and the heat flux $-\theta'(0)$ are decreased, while the value of free temperature $\theta(1)$ is increased which can be seen by the solution of both method and up to 4, 5 decimal place accuracy in the skin friction $f''(0)$, heat flux $-\theta'(0)$ and free temperature $\theta(1)$ take place shown in the concern table. In the next Table 7, increasing the value of Prandtl number Pr and decreasing the film thickness $\beta = \Upsilon^{\frac{1}{2}}$, increases the heat flux $-\theta'(0)$ and skin friction $f''(0)$ while decreases the free temperature $\theta(1)$ for the values of $A = 0.3$, $S = 0.4$, $Ma = 1$, $M = 1$ and $N = 0.2$. In both methods good accuracy are take place shown in Table 7. Similar observations are seen for the case when unsteady parameter S is increased and film thickness is reduced, then the heat flux $-\theta'(0)$ and skin friction $f''(0)$ are both increases up to some point and then decreases while free temperature $\theta(1)$ first decreases and then increases for $A = 0.3$, $Pr = 1$, $Ma = 1$, $M = 1$ and $N = 0.2$ as shown in the Table 8. Next Table 9 is for the case when Hartmann number Ma is increased and reducing the film thickness $\beta = \Upsilon^{\frac{1}{2}}$ then the skin friction $f''(0)$ and heat flux $-\theta'(0)$ both are decreases while interestingly free temperature $\theta(1)$ rises when the values of $A = 0.3$, $S = 0.4$, $Pr = 1$, $M = 1$ and $N = 0.2$ are used. Table 10 is the clear discussion about thermocapillary number M. By increasing thermocapillary number M will reduce the film thickness $\beta = \Upsilon^{\frac{1}{2}}$ and interestingly rises the free temperature $\theta(1)$ while both the skin friction $f''(0)$ and the value of heat flux $-\theta'(0)$ will decreases for the physical values of $A = 0.3$, $Pr = 1$, $Ma = 1$, $S = 0.4$ and $N = 0.2$. Good agreements are seen in the Table 10 for different values of the physical parameters between both methods.

The velocity and temperature profiles for variable viscosity and thermal conductivity hydromagnetics Newtonian flow under non-Isothermal condition over an unsteady stretching sheet are shown in Figs. 15–26 when A, N, S, Pr, Ma and M are varying for various values, respectively. By increasing the value of viscosity parameter A, flow velocity slowdown slightly and the temperature consistently rises as shown in Figs. 15 and 16. Here, it can be seen that the friction and velocity of fluid flow both are in opposite effects. when viscosity parameter increases so friction is increases, due to the fact that internal force of attraction increases which resist to the velocity of the molecule and hence velocity decreases consistently. As a result heat flux $-\theta'(0)$ decreases and free temperature $-\theta(1)$ increases, which is compatible with the physical phenomena. The effect of thermal conductivity parameter N on velocity field and temperature is shown in Figs. 17 and 18. It can be noticed, that when parameter N is increased the fluid velocity over the surface of stretching sheet with constant stretching parameters, $S = 0.4$, $A = 0.3$, $M = 1$, $Ma = 1$, $Pr = 1$ and $\Upsilon = 1.027013$ is decreased while temperature is increased. It means that when thermal conductivity increase then the flow of the fluid is slow down and the flow heats up and hence heat flux $-\theta'(0)$ and skin friction $f''(0)$ are decreased while free temperature $\theta(1)$ is increased. The effect of Prandtl number Pr (the ratio of momentum diffusivity towards thermal diffusivity), on velocity profile and temperature distribution are shown in Figs. 19 and 20. One can see in Fig. 20 that increasing Prandtl number Pr, the rate of heat transfer $-\theta'(0)$ slowdown and this decrease is seen in the whole domain of fluid, causes the flow become heated and the flow velocity is increased shown in Fig. 19. In Figs. 21 and 22 the effect of unsteady parameter S on velocity and temperature profiles are shown. It is clearly observed that when S is increased then the flow of the fluid speed up, and the flow of the fluid temperature consistently cools down. As a result heat flux $-\theta'(0)$ is increases in the boundary layer region, which is compatible with the physical phenomena. The effect of magnetic field on velocity field is shown in Fig. 23. It can be noticed, that increasing magnetic parameter Ma the fluid velocity over the surface of stretching sheet with constant stretching parameter, $S = 0.4$ increases. This is due to the fact that the presence of magnetic field provides Lorentz force because by repulsion which causes velocity increase. Similarly by increasing the magnitude of the magnetic field Ma, the temperature profile of the flow remain unchange as shown in Fig. 24. To observe the effectiveness of the surface tension gradient M (thermocapillary number), on velocity and temperature profiles Figs. 25 and 26 are plotted. With the increase of the thermocapillary number, the flow slowdown and the temperature remains

slightly unchange as shown in Figs. 25 and 26. Nusselt number $-\theta'(0)$ decreases due to the increase of the Thermocapillary number M which causes to the lower heat diffusivity on the stretching sheet thus the flow temperature unchange. Vibrating force remain constant in the flow molecules due to the temperature remain same (Fig. 27).

Concluding remarks

In this article, variable viscosity and thermal conductivity magneto hydrodynamic convection flow over the surface of unsteady stretching sheet with heat transfer under the effects of physical parameters are investigated. Two dimensional flow in the considered geometry is transformed into system of ODEs using specific transformations with meaning full geometry. For analysis couple of methods, BVP4C and HAM *mathematica* package **BVPh2.0** are used for comparison. Good agreements are observed during analysis of the both methods. The following results are concluded during this study:

1. It is found that by increasing A, the flow velocity slightly slow down and temperature rises consistently.
2. It is concluded that as N is increased the flow velocity is slow down while temperature is increased.
3. It is also concluded that with the increase of Prandtl number Pr, the flow speeds up while temperature decreases.
4. It is observed that by increasing S, the flow velocity increases, while temperature is decreases.
5. Moreover increasing Hartmann number Ma, the flow velocity strictly increases and temperature remains unchange.
6. It is also found that increasing the thermocapillary number M, the flow velocity decreases and no effect is observed on temperature.

Appendix A. Supplementary data

Supplementary data associated with this article can be found, in the online version, at https://doi.org/10.1016/j.rinp.2017.12.009.

References

[1] Crane LJ. Flow past a stretching plate. Z Angew Math Phys 1970;21:645–7.
[2] Wang CY. Liquid film on an unsteady stretching sheet. Q Appl Math 1990;48:601–10.
[3] Lai FC, Kulacki FA. The effect of variable viscosity on convective heat and mass transfer along a vertical surface in saturated porous media. Int J Heat Mass Trasfer 1991;33:1028–31.
[4] Andersson HI, Aarseth JB, Dandapat BS. Heat transfer in a liquid film on an unsteady stretching surface. Int J Heat Mass Transfer 2000;43:69–74.
[5] Wang C. Analytic solutions for a liquid thin film on an unsteady stretching surface. Heat Mass Transfer 2006;42:759–66.
[6] Seddeek MA, Salama FA. The effects of temperature dependent viscosity and thermal conductivtyon unsteady MHD convective heat transfer past a semi-infinite vertical porous moving plate with variable suction. Comp Mater Sci 2007;40:186–92.
[7] Liu IC, Andersson HI. Heat transfer in a liquid film on an unsteady stretching sheet. Int J Therm Sci 2008;47:766–72.
[8] Abel MS, Mahesha N, Tawade J. Heat transfer in a liquid film over an unsteady stretching surface with viscous dissipation in presence of external magnetic field. Appl Math Model 2009;33:3430–41.
[9] Dandapat BS, Santra B, Vajravelu K. The effects of variable fluid properties and thermocapillarity on the flow of a thin film on an unsteady stretching sheet. Int J Heat Mass Transfer 2007;50:991–6.
[10] Dandapat BS, Santra B, Andersson HI. Thermocapillarity in a liquid film on an unsteady stretching surface. Int J Heat Mass Transfer 2003;46:3009–15.
[11] Chen CH. Marangoni effects on forced convection of power-law liquids in a thin film over a stretching surface. Phys Lett A 2007;370:51–7.
[12] Khan Y, Qingbiao W, Faraz N, Yildirim A. The effect of variable viscosity and thermal conductivity on a thin film flow over a shrinking/stretching sheet. Comput Math Appl 2011;61:3391–9.
[13] Hazarika GC, Konch J. Effects of variable viscosity and thermal conductivity on magnatohydrodynamic forced convective boundary layer flow past a stretching/shrinking sheet prescribed with variable heat flux in the presence of heat source and constant suction. Int J Comp Appl 2014;107(1):8875–87.
[14] Dandapat BS, Maity S. Flow of a thin liquid film on an unsteady stretching sheet. Phys Fluids 2006;18:101–2.
[15] Dandapat BS, Kitamura A, Santra B. Transient film problem of thin liquid film flow on a stretching surface. Zeitschrift fur angewandte Mathematik und Physik 2006;57:623–35.
[16] Wang C, Pop I. Analysis of the flow of a power-law fluid film on an unsteady stretching surface by means of homotopy analysis method. J Non-Newtonian Fluid Mech 2006;138:161–72.
[17] Liao SJ. Beyond perturbation: introduction to homotopy analysis method. Chapman and Hall, Boca Raton 2004;336:1–67.
[18] Liao SJ. An optimal homotopy-analysis approach for strongly nonlinear differential equations, commun. Nonlinear Sci Numer Simul 2010;15:2003–16.
[19] Zhao Y, Liao S. HAM-based mathematica package BVPh 2.0 for nonlinear boundary value problems. In: Liao S, editor. Advances in the homotopy analysis method. World Scientific Press; 2013 [chapter 7].
[20] Rashidi MM, Momoniat E, Rostami B. Analytic approximate solutions for MHD boundary-layer viscoelastic fluid flow over continuously moving stretching surface by homotopy analysis method with two auxiliary parameters. J Appl Math 2012:19. Article ID 780415.
[21] Sharma RP, Avinash K, Sandeep N, Makinde OD. Thermal radiation effect on non-Newtonian fluid flow over a stretched sheet of non-uniform thickness. Defect Diffus Forum 2017;377:242–59.
[22] Beg OA, Bakier AY, Prasad VR. Numerical study of free convection magnetohydrodynamic heat and mass transfer from a stretching surface to a saturated porous medium with Soret and Dufour effects. Comput Mater Sci 2009;46(1):57–65.